Measurement of the Electron Magnetic Moment

X. Fan,[1, 2, *] T. G. Myers,[2] B. A. D. Sukra,[2] and G. Gabrielse[2, †]
[1]*Department of Physics, Harvard University, Cambridge, Massachusetts 02138, USA*
[2]*Center for Fundamental Physics, Northwestern University, Evanston, Illinois 60208, USA*
(Dated: September 28, 2022)

The electron magnetic moment in Bohr magnetons, $-\mu/\mu_B = 1.001\,159\,652\,180\,59\,(13)$ [0.13 ppt], is consistent with a 2008 measurement and is 2.2 times more precise. The most precisely measured property of an elementary particle agrees with the most precise prediction of the Standard Model (SM) to 1 part in 10^{12}, the most precise confrontation of all theory and experiment. The SM test will improve further when discrepant measurements of the fine structure constant α are resolved, since the prediction is a function of α. The magnetic moment measurement and SM theory together predict $\alpha^{-1} = 137.035\,999\,166\,(15)$ [0.11 ppb]

The quest to find physics beyond the Standard Model of Particle Physics (BSM) is well motivated because the SM is incomplete. No CP violation mechanism is large enough to keep matter and antimatter produced in the Big Bang [1] from annihilating as the universe cooled [2], dark matter [3, 4] has not been identified, and dark energy [5, 6] and inflation [7, 8] have no SM explanation. Great BSM sensitivity is afforded by the most precise prediction of the SM, the electron magnetic moment in Bohr magnetons, $-\mu/\mu_B = g/2$. SM sectors involved include the Dirac prediction [9], QED (quantum electrodynamics [10–17]) with muon and tauon contributions [18], along with hadronic [19–21] and weak interaction contributions [22–25]. BSM particles and electron substructure could make the measurement and prediction differ (like quark substructure shifts the proton moment).

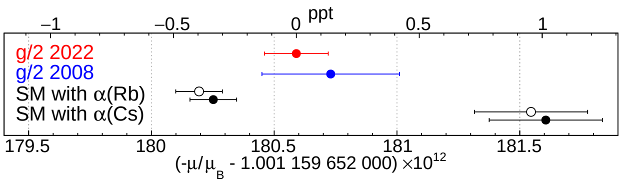

FIG. 1. This Northwestern measurement (red) and our 2008 Harvard measurement (blue) [26]. SM predictions (solid and open black points for slightly differing C_{10} [27, 28]) are functions of discrepant α measurements [29, 30]. A ppt is 10^{-12}.

The most precise determination of an elementary particle property, carried out blind of any prior measurement or prediction, gives μ/μ_B 2.2 times more precisely, to 1.3 parts in 10^{13} (Fig. 1). Measured in a new apparatus, it is consistent with the value that stood for 14 years [26]. In the most precise confrontation of theory and measurement, the SM prediction agrees to 1 part in 10^{12}. The measurement precision allows a much better SM test if discrepant measurements of the fine structure constant α [29, 30] are resolved, given that the SM prediction of μ/μ_B is a function of α.

The one-electron quantum cyclotron utilized is essentially a single electron suspended in a magnetic field $\mathbf{B} = B\hat{z}$ and cooled to its lowest quantum states [31]. The magnetic moment operator for a spin-1/2 electron,

$$\boldsymbol{\mu} = -\frac{g}{2}\,\mu_B\,\frac{\mathbf{S}}{\hbar/2}, \tag{1}$$

is proportional to its spin $\mathbf{S}$ normalized to its spin eigenvalue $\hbar/2$. For electron charge $-e$ and mass m, dimensional analysis gives a Bohr magneton, $\mu_B = e\hbar/(2m)$, as its approximate magnitude. The energy levels are

$$E = h\nu_s m_s + h\nu_c(n + \tfrac{1}{2}), \tag{2}$$

with $h = 2\pi\hbar$, $m_s = \pm 1/2$ and $n = 0, 1, ...$ The cyclotron frequency is $\nu_c = eB/(2\pi m)$, the spin frequency is $\nu_s = (g/2)\nu_c$, and the anomaly frequency is $\nu_a \equiv \nu_s - \nu_c$. The electron serves as its own magnetometer insofar as

$$-\frac{\mu}{\mu_B} = \frac{g}{2} = 1 + \frac{\nu_a}{\nu_c} \tag{3}$$

is independent of B, which cancels out in ν_a/ν_c.

A stable magnetic field is nonetheless critical for ν_a and ν_c not measured simultaneously. Field drift reduced by a factor of 4 to 2×10^{-9}/day [32] makes possible round-the-clock measurements, improved statistical precision, and a better investigation of uncertainties. The apparatus in Fig. 2a achieves this by supporting a 50 mK electron trap on a 4.2 K superconducting, self-shielding solenoid [33], with a mixing chamber flexibly hanging from the rest of a dilution refrigerator [34]. (Independently suspending a trap and a normal rigid fridge makes B drift with lab pressure and temperature as the electron moves in the slight gradient of the solenoid field [35].) The He and N_2 pressures in the cryostats are also regulated.

An electron in the field $B\hat{z}$ is trapped by adding an electrostatic quadrupole potential $V \propto z^2 - \rho^2/2$, with $\boldsymbol{\rho} = x\hat{\mathbf{x}} + y\hat{\mathbf{y}}$ [36]. Cylindrical Penning trap electrodes [37, 38] (Fig. 2b) are shaped so that properly biasing produces such a potential. A centered electron then oscillates nearly harmonically along $\hat{z}$ at the axial frequency $\bar{\nu}_z \approx 114$ MHz. For $B = 5.3$ T, the trap-modified cyclotron and anomaly frequencies are $\bar{\nu}_c \approx 149$ GHz and $\bar{\nu}_a \approx 173$ MHz, while ν_s is unchanged. A circular magnetron motion at $\bar{\nu}_m = 43$ kHz is cooled by axial sideband cooling [36, 39] and not discussed further. Figure 2c

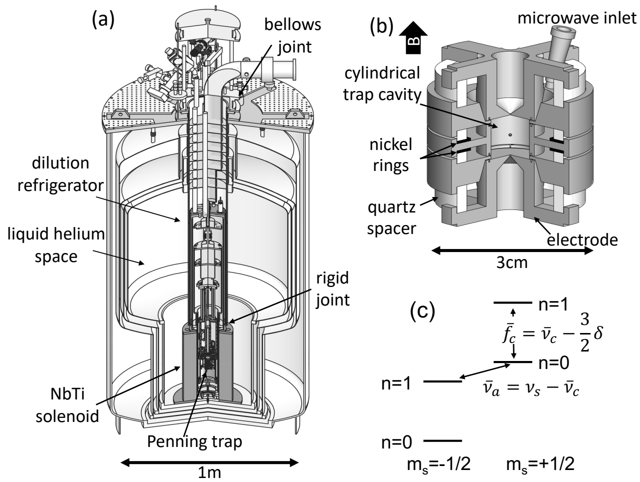

FIG. 2. (a) Cryogenic system supports a 50 mK electron trap upon a 4.2 K solenoid to provide a very stable B. (b) Silver electrodes of a cylindrical Penning trap. (c) Quantum spin and cyclotron energy levels used for measurement.

shows the lowest cyclotron and spin energy levels and the frequency spacings. A relativistic mass shift δ is given by $\delta/\nu_c \equiv h\nu_c/(mc^2) \approx 10^{-9}$ [36, 40].

The lowest cyclotron states for each spin are effectively stable because the spin is so nearly uncoupled from its environment [36]. With no trap, the excited cyclotron state lifetime is 0.1 s. In the trap, the rate for spontaneous emission of synchrotron radiation is inhibited by a factor of 50 to 70, when B is chosen so $\bar{\nu}_c$ is far from resonance with cavity radiation modes [41]. Seconds of averaging time allows a cyclotron excitation to be detected before it decays [35]. The cyclotron damping contributes 0.03 Hz to the cyclotron and anomaly linewidths (to be discussed), a negligible 0.2 ppt and a very important 0.2 ppb, respectively. Blackbody photons that could excite the electron from the cyclotron ground state are eliminated for a trap cavity cooled below 100 mK [31].

The Brown-Gabrielse invariance theorem [42],

$$\nu_c = \sqrt{\bar{\nu}_c^2 + \bar{\nu}_z^2 + \bar{\nu}_m^2} \tag{4}$$

provides the ν_c and $\nu_a = \nu_s - \nu_c$ needed in Eq. (3) to get μ/μ_B in terms of the trap-modified frequencies and $\bar{\nu}_a \equiv \nu_s - \bar{\nu}_c$. It is critical that Eq. (4) is invariant under unavoidable misalignments of $\mathbf{B}$ and the axis of V, and under elliptic distortions of V [42]. The hierarchy $\bar{\nu}_c \gg \bar{\nu}_z \gg \bar{\nu}_m \gg \delta$ allows an expansion of Eq. (4) that suffices for our precision to be inserted in Eq. (3) to obtain

$$-\frac{\mu}{\mu_B} = \frac{g}{2} \simeq 1 + \frac{\bar{\nu}_a - \bar{\nu}_z^2/(2\bar{f}_c)}{\bar{f}_c + 3\delta/2 + \bar{\nu}_z^2/(2\bar{f}_c)} + \frac{\Delta g_{cav}}{2}, \tag{5}$$

with $\bar{\nu}_a$ and $\bar{f}_c$ (defined in Fig. 2c) deduced with $\bar{\nu}_z$ from measured line shapes (Fig. 3). The added cavity-shift $\Delta g_{cav}/2$ arises because couplings to radiation modes of the trap cavity shift $\bar{\nu}_c$ [43, 44].

To measure the axial frequency $\bar{\nu}_z$ needed in Eq. (5), a resonant circuit that is the input for a cryogenic HEMT amplifier is attached to the trap electrodes. The dissipation of current induced in the circuit by electron axial motion damps it with a time constant $\gamma_z^{-1} = 32$ ms. The amplifier heats the electron axial motion to $T_z = 0.5$ K. The 1-minute Fourier transform of the amplifier output in Fig. 3c shows the noise and electron signal canceling to make a dip that reveals $\bar{\nu}_z$ [45].

Small shifts in $\bar{\nu}_z$ provide quantum nondemolition (QND) detection of one-quantum spin and cyclotron jumps, without the detection changing the cyclotron or spin state. Saturated nickel rings (Fig. 2b) produce a magnetic bottle gradient, $\Delta B = B_2\left[(z^2 - \rho^2/2)\hat{z} - z\rho\hat{\rho}\right]$ with $B_2 = 300$ T/m^2. This couples spin and cyclotron energies to $\bar{\nu}_z$ which then shifts by $\Delta\bar{\nu}_z \approx 1.3\,(n{+}m_s)$ Hz. The B_2 and $\Delta\bar{\nu}_z$ are 5 and 3 times smaller than used previously [26]. To rapidly detect jumps after the cyclotron and anomaly drives are turned off, the amplified signal is immediately fed back to the electron. This self-excited oscillator (SEO) [46] is resonantly and rapidly driven to a large amplitude, even if $\bar{\nu}_z$ shifts with amplitude, whereupon the gain is adjusted to maintain it. A Fourier transform of the large signal reveals the small $\Delta\bar{\nu}_z$ that signals single cyclotron and spin quantum jumps.

Quantum jump spectroscopy produces anomaly and cyclotron resonances (Fig. 3a-b) from which to extract $\bar{\nu}_a$ and $\bar{f}_c$ to use in Eq. (5). Cyclotron and anomaly quantum jump trials are alternated. The magnetic field drift of 0.2 ppb/hr in the new apparatus is slow enough that we can correct the magnetic field using a quadratic fit to the lowest cyclotron drive frequency that produced an excitation. Each trial starts with the electron in the spin-up ground state, $|n=0, m_s=1/2\rangle$, and 5 s of axial magnetron sideband cooling [36, 39].

To produce cyclotron quantum jumps, a 5 s microwave drive is injected between trap electrodes (Fig. 2b) to produce quantum jumps to $n_c = 1$ less than 20% of the trials, to avoid saturation effects. An anomaly drive is also applied but is off resonance. Cavity-inhibited spontaneous emission [41] allows the excitation to persist long enough so that during the next 1 s we can switch on the self-excitation feedback [46] and detect the 1.3 Hz shifts that signal cyclotron quantum jumps.

To produce anomaly quantum jumps, an oscillatory potential applied to trap electrodes for 30 s drives an off-resonance axial oscillation of the electron through the radial magnetic gradient $B_2 z\boldsymbol{\rho}$. (A cyclotron drive remains applied but is off resonance). The electron sees an oscillating magnetic field perpendicular to $\hat{z}$ as needed to flip its spin, with a radial gradient that allows a simultaneous cyclotron transition [36]. A spontaneous decay to the spin-down ground state, $|n=0, m_s=-1/2\rangle$, would be detected during the 60 s (more than 10 cyclotron decay times) after drives are turned off. A maximum quantum jump rate of 40% suggests a slight power broadening, but $\bar{\nu}_a$ is still determined far more precisely than $\bar{f}_c$.

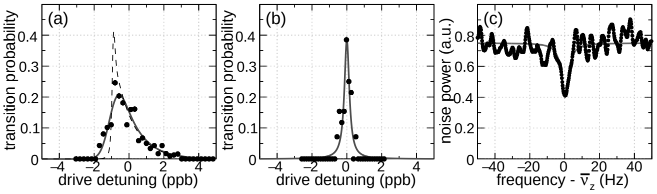

FIG. 3. Quantum jump cyclotron (a) and anomaly (b) line shapes that are measured (points), predicted (dashed) and fit (solid) vs fractional drive detunings from $\bar{f}_c(1+\epsilon)$ and $\bar{\nu}_a(1+\epsilon)$. (c) A dip in a noise resonance is fit to get $\bar{\nu}_z$.

Asymmetric anomaly and cyclotron line shapes are well understood [47], and the effect of cyclotron decay can be added [35]. Thermal axial motion through the gradient, $B_2 z^2$, gives both lines a fractional width, $\epsilon = B_2 k_B T_z/(4\pi^2 \bar{\nu}_z^2 m B)$ with Boltzmann constant k_B. The anomaly width $\epsilon\bar{\nu}_a$ corresponds to establishing $\bar{\nu}_a$ in 1.1 s, much longer than the $\gamma_z^{-1} = 32$ ms required for axial energy changes. Averaging thus produces a much narrower peak, nearly symmetric about the frequency $\bar{\nu}_a(1+\epsilon)$ for the average field the electron sees. Of the remaining observed 0.06 Hz (0.35 ppb) linewidth, half is from cyclotron decay and half from the limited 30 s time the anomaly drive is applied. The 1.3 ms cyclotron averaging is much shorter than $\gamma_z^{-1} = 32$ ms so the cyclotron line shape mostly reflects a Boltzmann distribution of axial energies (dashed in Fig. 3a), with negligible broadening from cyclotron decay and drive duration.

Magnetic field fluctuations from other sources would also be averaged differently in the observed anomaly and cyclotron line shapes. Such fluctuations, with a 200 Hz bandwidth, were observed with a superconducting solenoid being jostled by its environment [48]. The anomaly line shape would average away such fluctuations to yield a narrow linewidth as is observed (e.g. Fig. 3b). The cyclotron line shape would not average away such such fluctuations, which are thus a possible explanation for the observed 0.5–0.8 ppb broadening (e.g. Fig. 3a).

Both $\bar{\nu}_a$ and $\bar{f}_c$ are extracted from the line shapes. Cyclotron line shapes are fit to the predicted line shape (dashed in Fig. 3a), convoluted with a Gaussian function to accommodate the broadening. Such a fit, illustrated by the solid curve in Fig. 3a, typically gives a 2 ppb cyclotron linewidth, a Gaussian broadening width of about 0.5 ppb, a $T_z = 0.55 \pm 0.11$ K, and a $\bar{f}_c$ with an uncertainty of about 0.08 ppb. The much more symmetric anomaly line shapes (e.g. Fig. 3b) are fractionally narrower by about a factor of 4. Since uncertainty in $\bar{\nu}_a$ is thus not very significant for our final uncertainty, fitting with or without Gaussian broadening makes little difference (e.g. solid curve in Fig. 3b).

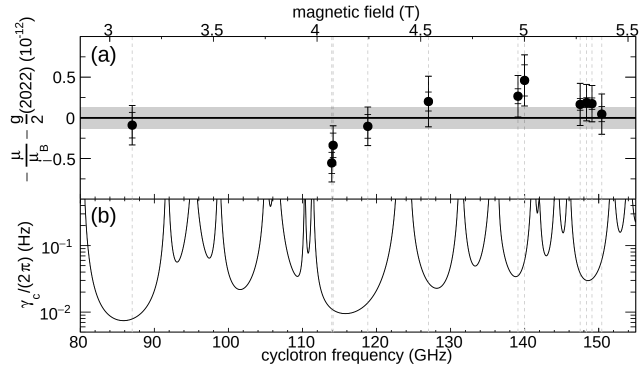

FIG. 4. (a) Measured $-\mu/\mu_B - g/2$ after cavity-shift correction. (b) Measurements take place in valleys of the cyclotron damping rate where spontaneous emission is inhibited.

The cavity-shift $\Delta g_{cav}/2$ in Eq. (5), the only correction to what is directly measured, arises because $\bar{\nu}_c$ shifts because the cyclotron oscillator couples to radiation modes of the trap cavity [43, 44]. It is the downside of the cavity-inhibited spontaneous emission that desirably narrows resonance lines, and makes it possible to observe a cyclotron excitation before it decays. The cylindrical trap was invented [37] to allow cavity modes and shifts to be understood and calculated. Nonetheless, the mode frequencies and Q values must still be measured because the cavity is imperfectly machined, is slit to make cavity sections into separately-biased trap electrodes, and its dimensions change as it cools below 100 mK from 300 K. Three consistent methods are used: (1) parametrically-pumped electrons [35, 49, 50], (2) measuring how long one electron stays in its first excited cyclotron state [26, 35], and (3) a new method of observing the decay time of an electron exited to $n_c \approx 10$.

A renormalized calculation [43, 44] with added cyclotron damping [26, 35] avoids the infinite cavity shifts that result from summing all mode contributions. This calculation assumes the mode frequencies of a perfect cylinder, one Q for TE modes, and another for TM modes. We calculate with dimensions chosen to best match observed frequencies and a single Q value for all modes. After shifts from the 72 observed modes using the ideal frequencies and the one Q value are subtracted out, contributions for these modes using measured frequencies and Q values are added back in. The leading contribution to cavity shift uncertainties comes from modifications of the field that an electron sees from imperfections and misalignments of the trap cavity. Figure 4a shows the consistency of μ/μ_B measurements at 11 different magnetic fields, after each receives a different cavity shift.

A weighted average of the 11 measurements gives

$$\frac{g}{2} = 1.001\,159\,652\,180\,59\,(13) \quad [0.13 \text{ ppt}], \qquad (6)$$

with 1σ uncertainty in the last two digits in parentheses.

TABLE I. Largest uncertainties for $g/2$.

Source	**Uncertainty**$\times 10^{13}$
statistical	0.29
cyclotron broadening	0.94
cavity correction	0.90
nuclear paramagnetism	0.12
anomaly power shift	0.10
magnetic field drift	0.09
total	1.3

(This is a 3100 times higher precision than achieved with muon moments [51]). Figure 1 shows the good agreement of this 2022 measurement at Northwestern with our 2008 measurement at Harvard [26] and an uncertainty that is improved by a factor of 2.2. Because similar measurement methods were used, we do not recommend averaging the two measurements because similar methods may produce correlated uncertainties that are difficult to determine. Table I lists uncertainty contributions to the final result, with correlations taken into account. The statistical uncertainty is from the fits that extract $\bar{f}_c$ and $\bar{\nu}_a$. The two dominant uncertainties have been discussed – cyclotron broadening and cavity shifts (treated as correlated for nearby fields). The measured temperature variations of the silver electrodes determines the uncertainty from their nuclear paramagnetism. The anomaly power shift uncertainty comes from the measured frequency dependence on drive strength. The field drift uncertainty is from the fit to the slowly drifting field.

Several SM sectors together predict

$$\frac{g}{2} = 1 + C_2\left(\frac{\alpha}{\pi}\right) + C_4\left(\frac{\alpha}{\pi}\right)^2 + C_6\left(\frac{\alpha}{\pi}\right)^3 + C_8\left(\frac{\alpha}{\pi}\right)^4 + C_{10}\left(\frac{\alpha}{\pi}\right)^5 + \ldots + a_{\mu\tau} + a_{\text{hadronic}} + a_{\text{weak}}. \qquad (7)$$

The Dirac prediction [9] is first on the right. QED provides the asymptotic series in powers of the fine structure constant α, and the muon and tauon contribution $a_{\mu\tau}$ [27]. The constants C_2 [10], C_4 [11, 12], C_6 [13, 14] and C_8 [15] are calculated exactly, but require measured lepton mass ratios as input [18]. The measurements are so precise that a numerically calculated tenth order C_{10} [16, 17] is required and tested. A second evaluation of C_{10} [28] differs slightly for reasons not yet understood and the open points in Figs. 1 and 5 use this alternative. Hadronic and weak interaction contributions are a_{hadronic} [19–21] and a_{weak} [22–25]. The exact C_8 and the numerical C_{10} are remarkable advances that reduce the calculation uncertainty well below the uncertainties reported for the measured μ/μ_B and α.

The most precise α measurements [29, 30], needed for the SM prediction of $g/2$ from Eq. (7), disagree by 5.5 σ, nearly ten times our measurement uncertainty (Fig. 1). Until the discrepancy is resolved, the best that can be said is that the predicted and measured μ/μ_B agree to about $\delta(g/2) = 0.7 \times 10^{-12}$, half of the α discrepancy. A generic chiral symmetry model [52] then suggests that the electron radius is less than $R_e = \sqrt{|\delta(g/2)|\hbar/(mc)} = 3.2 \times 10^{-19}$ m, and that the mass of possible electron constituents must exceed $m^* = m/\sqrt{|\delta(g/2)|} = 620$ GeV$/c^2$.

If the α discrepancy and uncertainty would be reduced so $\delta(g/2)$ equals our μ/μ_B measurement uncertainty, then R_e reduces to 1.4×10^{-19} m and m^* increases to 1.4 TeV$/c^2$. A further reduction of $\delta(g/2)$ by only a factor of 2.3 would bring us to the level of the current discrepancy between the calculated and measured muon magnetic moments [51, 53], presuming that it is due to BSM physics that is smaller for the electron by a factor of the square of the ratio of the two masses.

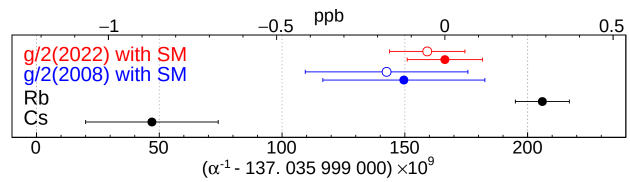

FIG. 5. SM prediction of α using μ/μ_B from this Northwestern measurement (red), and from our 2008 Harvard measurement (blue), with solid and open points for slightly differing C_{10} [27, 28]. The α measurements (black) made with Cs at Berkeley [29] and Rb in Paris [30]. A ppb is 10^{-9}.

The fine structure constant α is the fundamental measure of the strength of the electromagnetic interaction in the low energy limit. For the SI system of units, $\alpha = e^2/(4\pi\epsilon_0\hbar c)$ is a measure of the vacuum permittivity ϵ_0, given that and e, $\hbar$ and the speed of light c are now defined [54]. Our measured μ/μ_B and the SM give

$$\begin{aligned}\alpha^{-1} &= 137.035\,999\,166\,(02)\,(15) \quad [0.014 \text{ ppb}]\,[0.11 \text{ ppb}],\\ &= 137.035\,999\,166\,(15) \qquad [0.11 \text{ ppb}], \qquad (8)\end{aligned}$$

with theoretical and experimental uncertainties in the first and second brackets. Figure 5 compares to the α measurements (black) that disagree with each other by 5.5 σ. Our value differs by 2.1 standard deviations from the Paris Rb determination of α [30] and by 3.9 standard deviations from the Berkeley Cs determination [29]. The C_{10} in [28] would change only “66” to “59” in Eq. (8).

For the future, a measurement is underway to realize the new precision with a positron, to improve the test the fundamental CPT symmetry invariance of the SM by a factor of 40 [55]. Much larger improvements in the precision of μ/μ_B now seem feasible given the demonstration of more stable apparatus, improved statistics, and better understood uncertainties. Detectors being tested, more harmonic and lower loss trap cavities, and detector backaction circumvention methods [56, 57] should enable much more precise measurements to come.

In conclusion, an electron magnetic moment measurement is carried out blind to previous measurements and predictions. A PhD thesis [58] and a longer publication in preparation give fuller accounts. In new apparatus at a different university, the measured μ/μ_B is consistent with our 2008 measurement, with a factor of 2.2 improved precision. The most precise prediction of the SM agrees with the most precise determination of a property of an elementary particle to about 1 part in 10^{12}. When discrepant α measurements are resolved, the new measurement uncertainty of 1.3 parts in 10^{13} is available for a much more precise test for BSM physics

Early contributions were made by S. E. Fayer. NSF provided the support, with X. Fan supported by the Masason Foundation. Detector development is supported by the Templeton Foundation, and low-loss trap cavity development is supported by the DOE SQMS Center.

---

* xing.fan@northwestern.edu
† gerald.gabrielse@northwestern.edu

[1] G. Gamow, Phys. Rev. **70**, 572 (1946).
[2] A. D. Sakharov, Soviet Journal of Experimental and Theoretical Physics Letters **5**, 24 (1967).
[3] F. Zwicky, Helvetica Physica Acta **6**, 110 (1933).
[4] V. C. Rubin, J. Ford, W. K., and N. Thonnard, Astrophys. J.**238**, 471 (1980).
[5] S. Perlmutter *et al.*, The Astrophysical Journal **517**, 565 (1999).
[6] A. G. Riess *et al.*, The Astronomical Journal **116**, 1009 (1998).
[7] A. Friedman, Zeitschrift für Physik **10**, 377 (1922).
[8] G. Lemaître, Annales de la Société scientifique de Bruxelles **47**, 49 (1927).
[9] P. A. M. Dirac, Proceedings of the Royal Society of London Series A **118**, 351 (1928).
[10] J. Schwinger, Phys. Rev. **73**, 416 (1948).
[11] A. Petermann, Helv. Phys. Acta **30**, 407 (1957).
[12] C. M. Sommerfield, Ann. Phys. (N.Y.) **5**, 26 (1958).
[13] T. Kinoshita, Phys. Rev. Lett. **75**, 4728 (1995).
[14] S. Laporta and E. Remiddi, Phys. Lett. B **379**, 283 (1996).
[15] S. Laporta, Physics Letters B **772**, 232 (2017).
[16] T. Aoyama, T. Kinoshita, and M. Nio, Phys. Rev. D **97**, 036001 (2018).
[17] T. Aoyama, M. Hayakawa, T. Kinoshita, and M. Nio, Phys. Rev. Lett. **109**, 111807 (2012).
[18] A. Kurz, T. Liu, P. Marquard, and M. Steinhauser, Nuclear Physics B **879**, 1 (2014).
[19] D. Nomura and T. Teubner, Nucl. Phys. B **867**, 236 (2013).
[20] A. Kurz, T. Liu, P. Marquard, and M. Steinhauser, Physics Letters B **734**, 144 (2014).
[21] Jegerlehner, Fred, EPJ Web Conf. **218**, 01003 (2019).
[22] K. Fujikawa, B. W. Lee, and A. I. Sanda, Phys. Rev. D **6**, 2923 (1972).
[23] A. Czarnecki, B. Krause, and W. J. Marciano, Phys. Rev. Lett. **76**, 3267 (1996).
[24] M. Knecht, M. Perrottet, E. de Rafael, and S. Peris, Journal of High Energy Physics **11**, 003 (2002).
[25] A. Czarnecki, W. J. Marciano, and A. Vainshtein, Phys. Rev. D **67**, 073006 (2003).
[26] D. Hanneke, S. Fogwell, and G. Gabrielse, Phys. Rev. Lett. **100**, 120801 (2008).
[27] T. Aoyama, T. Kinoshita, and M. Nio, Atoms **7**, 28 (2019).
[28] S. Volkov, Phys. Rev. D **100**, 096004 (2019).
[29] R. H. Parker, C. Yu, W. Zhong, B. Estey, and H. Müller, Science **360**, 191 (2018).
[30] L. Morel, Z. Yao, P. Cladé, and S. Guellati-Khélifa, Nature **588**, 61 (2020).
[31] S. Peil and G. Gabrielse, Phys. Rev. Lett. **83**, 1287 (1999).
[32] X. Fan, S. E. Fayer, and G. Gabrielse, Review of Scientific Instruments **90**, 083107 (2019).
[33] G. Gabrielse and J. Tan, J. Appl. Phys. **63**, 5143 (1988).
[34] G. Gabrielse, S. Fayer, T. Myers, and X. Fan, Atoms **7**, 45 (2019).
[35] D. Hanneke, S. Fogwell Hoogerheide, and G. Gabrielse, Phys. Rev. A **83**, 052122 (2011).
[36] L. S. Brown and G. Gabrielse, Rev. Mod. Phys. **58**, 233 (1986).
[37] G. Gabrielse and F. C. MacKintosh, Intl. J. of Mass Spec. and Ion Proc. **57**, 1 (1984).
[38] J. Tan and G. Gabrielse, Appl. Phys. Lett. **55**, 2144 (1989).
[39] R. S. Van Dyck, Jr., P. B. Schwinberg, and H. G. Dehmelt, in *New Frontiers in High Energy Physics*, edited by B. Kursunoglu, A. Perlmutter, and L.Scott (Plenum, New York, 1978), p. 159.
[40] G. Gabrielse, H. Dehmelt, and W. Kells, Phys. Rev. Lett. **54**, 537 (1985).
[41] G. Gabrielse and H. Dehmelt, Phys. Rev. Lett. **55**, 67 (1985).
[42] L. S. Brown and G. Gabrielse, Phys. Rev. A **25**, 2423 (1982).
[43] L. S. Brown, G. Gabrielse, K. Helmerson, and J. Tan, Phys. Rev. Lett. **55**, 44 (1985).
[44] L. S. Brown, G. Gabrielse, K. Helmerson, and J. N. Tan, Phys. Rev. A **32**, 3204 (1985).
[45] D. J. Wineland and H. G. Dehmelt, J. Appl. Phys. **46**, 919 (1975).
[46] B. D'Urso, R. Van Handel, B. Odom, D. Hanneke, and G. Gabrielse, Phys. Rev. Lett. **94**, 113002 (2005).
[47] L. S. Brown, Ann. Phys. (N.Y.) **159**, 62 (1985).
[48] J. W. Britton, J. G. Bohnet, B. C. Sawyer, H. Uys, M. J. Biercuk, and J. J. Bollinger, Phys. Rev. A **93**, 062511 (2016).
[49] J. Tan and G. Gabrielse, Phys. Rev. A **48**, 3105 (1993).
[50] J. Tan and G. Gabrielse, Phys. Rev. Lett. **67**, 3090 (1991).
[51] B. Abi *et al.*, Phys. Rev. Lett. **126**, 141801 (2021).
[52] S. J. Brodsky and S. D. Drell, Phys. Rev. D **22**, 2236 (1980).
[53] T. Aoyama *et al.*, Physics Reports **887**, 1 (2020).
[54] M. Stock, R. Davis, E. de Mirandés, and M. J. T. Milton, Metrologia **56**, 022001 (2019).
[55] S. Fogwell Hoogerheide, J. C. Dorr, E. Novitski, and G. Gabrielse, Review of Scientific Instruments **86**, 053301 (2015).
[56] X. Fan and G. Gabrielse, Phys. Rev. Lett. **126**, 070402 (2021).
[57] X. Fan and G. Gabrielse, Phys. Rev. A **103**, 022824 (2021).
[58] X. Fan, Ph.D. thesis, Harvard University, 2022, (thesis

advisor: G. Gabrielse).